Received: 5 December 2024 | Revised: 17 February 2025 | Accepted: 18 March 2025

DOI: 10.1096/fj.202403111R

RESEARCH ARTICLE

The FASEB Journal

Construction and diagnostic efficacy assessment of the urinary exosomal miRNA-mRNA network in children with IgA vasculitis nephritis

Yunfan Zhang[1,2] | Huanhuan Yang[1,2] | Yi Chen[2] | Yuxian Tang[1,2] | Junyan Chen[2] | Jun Huang[2] | Ai Feng[2] | Zengfeng Weng[2] | Fenrong Li[2] | Jinfeng Lin[2] | Jingqi Xie[2] | Chunfang Zhang[2] | Jie Chen[3] | Chunlin Gao[4] | Xiaojing Nie[1,3,5]

[1]Department of Pediatrics, Fuzong Clinical Medical College of Fujian Medical University, Fuzhou, China

[2]Department of Pediatrics, 900th Hospital of PLA Joint Logistic Support Force, Fuzhou, China

[3]Department of Pediatrics, Fujian Provincial Hospital, Fuzhou, China

[4]Department of Pediatrics, Jinling Hospital, Medical School of Nanjing University, Nanjing, China

[5]Department of Pediatrics, Dongfang Hospital of Xiamen University, School of Medical, Xiamen University, Fuzhou, China

Correspondence
Xiaojing Nie, No. 156 Xi Er Huan Bei Road, Fuzhou 350025, Fujian Province, China.
Email: searchnj051@126.com

Funding information
Science and Technology Innovation Project of Fujian Province, Grant/Award Number: 2019Y9043; Key Project of Social Development of Fujian Province of China, Grant/Award Number: 2019Y0069 and 2023Y0068

Abstract

This study aimed to comprehensively evaluate the diagnostic potential of urinary exosomal microRNA (miRNA) in IgA vasculitis (IgAV) kidney injury by meticulously comparing the miRNA expression profiles in urine exosomes between children diagnosed with IgAV and those with IgA vasculitis nephritis (IgAVN). Urine samples were obtained from children with IgAV who were treated at our hospital from October 2022 to October 2023. These samples were then categorized into the IgAV group and the IgAVN group. High-throughput sequencing and bioinformatics analysis techniques were employed to conduct a thorough analysis of the differentially expressed miRNAs between the two groups. Additionally, the correlation between urinary exosomal miRNA and clinical parameters was evaluated. A total of 57 urinary exosomal miRNAs exhibited differential expression between the IgAV and IgAVN groups. Specifically, in the IgAVN group, 42 miRNAs were upregulated, while 15 were downregulated. Lasso regression analysis and ROC analysis identified five candidate urinary exosomal miRNAs with high diagnostic accuracy. A prediction of 95 target genes related to the candidate miRNAs led to the construction of an exosomal miRNA-mRNA regulatory network consisting of four key miRNAs and ten hub genes. Gene function and metabolic pathway analyses indicated that these ten hub genes were predominantly enriched in pro-fibrotic and inflammatory pathways. The analysis incorporating clinical parameters demonstrated a significant correlation between hsa-miR-383-5p and urinary protein levels. This research identified exosomal miRNAs and mRNAs with differential expression patterns associated with IgAVN and constructed the corresponding exosomal miRNA-mRNA network. It was determined that

Yunfan Zhang and Huanhuan Yang contributed equally to this work.

hsa-miR-3065-5p, hsa-miR-383-5p, hsa-miR-25-3p, and hsa-miR-450b-5p might mediate the pathogenesis of IgAVN by targeting pro-fibrotic and inflammatory pathways. Among them, exosomal hsa-miR-383-5p is highly likely to serve as a novel non-invasive biomarker for assessing the disease status of IgAVN, thereby offering new perspectives on the non-invasive diagnosis and treatment of IgAVN.

KEYWORDS

exosomes, hsa-miR-383-5p, IgA vasculitis, IgA vasculitis nephritis, miRNA

1 | INTRODUCTION

IgA vasculitis (IgAV), the most prevalent systemic small-vessel vasculitis in childhood, has an annual incidence of 3–27 cases per 100 000 population.[1,2] It is characterized by the deposition of IgA-dominant immune complexes and the activation of neutrophils surrounding small vessels.[1,2] IgAV has the potential to affect multiple systems, and approximately 20%–80% of affected children develop kidney damage within 4–6 weeks after the onset, which is defined as IgA vasculitis with nephritis (IgAVN).[3,4] Additionally, 1%–7% of children with IgAVN may progress to end-stage kidney disease, suggesting that the severity of kidney involvement plays a decisive role in the long-term prognosis of IgAV.[3,4]

The gold standard for the diagnosis of IgAVN is renal biopsy, an invasive procedure that is often difficult for parents to accept. Consequently, in clinical practice, the diagnosis predominantly hinges on laboratory indicators including urinalysis, urinary phase contrast, 24-h urinary protein quantification, and the urinary protein/creatinine ratio.[5] Nevertheless, these indicators exhibit a lag effect and are unable to predict the onset of IgA nephropathy at an early stage, thus necessitating the development of novel, specific non-invasive markers for the diagnosis of IgAVN.

Recent investigations have reported various blood and urine biomarkers potentially enabling the early prediction of IgAV-related renal injury. These biomarkers encompass galactose-deficient IgA1 (Gd-IgA1), apolipoprotein M (ApoM), kidney injury molecule-1 (KIM-1), monocyte chemoattractant protein-1 (MCP-1), and angiotensinogen (AGT).[5–7] Nevertheless, these biomarkers necessitate further clinical validation. Moreover, urinary exosomes, originating from renal epithelial cells, have emerged as a promising area of research. This is attributed to their rich miRNA content and potential applicability in targeting the root causes of renal injury.[8,9] In this context, the current study aims to assess the feasibility of using urinary exosomal miRNA as a diagnostic means for evaluating kidney injury in children with IgAV, with the ultimate goal of improving patient prognosis.

2 | METHODS

2.1 | Subjects

Samples were collected from five children with IgAV and five children with IgAVN at 900th Hospital of PLA Joint Logistic Support Force between October 2022 and October 2023. For IgAV, the inclusion criteria stipulated that patients had to meet the classification criteria for IgAV established by EULAR/PRINTO/PReS in 2008. Regarding IgAVN, the inclusion criteria required patients to meet the diagnostic criteria delineated in the "Evidence-based Guidelines for the Diagnosis and Treatment of Henoch-Schönlein Purpura Nephritis (2016)". The exclusion criteria were as follows: patients with a history of primary or other secondary kidney diseases, such as nephrotic syndrome, chronic glomerulonephritis, IgA nephropathy, thin basement membrane disease, hepatitis B virus-associated nephritis; or those with a history of immune system diseases like Kawasaki disease, systemic lupus erythematosus; or those with a history of taking nephrotoxic drugs. Informed consent was duly obtained from all parents, who signed the consent forms. This study was approved by the Ethics Committee of 900th Hospital of PLA Joint Logistic Support Force (Nos. 2020-071 and 2023-081).

2.2 | Data collection

Gather demographic and clinical data from the study subjects, encompassing age, gender, blood biochemistry parameters, 24-h urinary protein levels, urinary red blood cell counts, renal pathology findings, as well as morning urine samples.

2.3 | Urine exosome isolation

A total of 40 mL of morning urine sample was obtained from each patient, and exosome separation was immediately performed on each sample after collection. Urine samples were subjected to centrifugation at 4°C and 3000×*g* for 10 min. The resultant supernatant was carefully transferred into a new sterile centrifuge tube. Subsequently, this supernatant underwent another centrifugation step at 2000×*g* and 4°C for 30 min. Following this, the supernatant was transferred to a fresh centrifuge tube and centrifuged once more at 10 000×*g* and 4°C for 45 min to eliminate larger vesicles. Next, the supernatant was filtered through a 0.45 μm filter membrane, and the filtrate was collected into a new centrifuge tube. Subsequently, the filtrate was ultra centrifuged at 100 000×*g* and 4°C for 70 min. After discarding the supernatant, the pellet was resuspended in 10 mL of pre-chilled 1×PBS buffer and then centrifuged again under identical conditions for 70 min. Finally, the supernatant was removed, and the pellet, composed of the isolated exosomes, was resuspended in 250 μL of pre-chilled 1×PBS buffer and stored at −80°C. One of the samples was selected for further observation of exosomes under transmission electron microscopy (TEM), particle size analysis, and exosome marker protein detection.

2.4 | TEM observation of exosome structure

Aliquot 10 μL of the exosome resuspension and place it on a 2 mm diameter copper grid to allow for precipitation over a period of 1 min. Subsequently, with care, use filter paper to blot the residual liquid from the edge of the copper grid. Next, apply 10 μL of uranyl acetate to the copper grid, permit it to precipitate for 1 min, and then use filter paper to wick away the excess stain. After air-drying at room temperature for a few minutes, visualize the exosome structure under a TEM (HT7700/HITACHI, Tokyo, Japan) operating at 100 kV and capture images.

2.5 | Analysis of exosome particle size

Aliquot 10 μL of the exosome resuspension and dilute it to a final volume of 30 μL. Initially, conduct an instrument performance test using standard samples. Once the instrument is qualified, proceed with loading the exosome sample. Employ the particle sizer (N30E/NanoFCM, Fujian, China) to determine the particle size and concentration details of the exosomes.

2.6 | Identification of exosome marker protein

Characterize the exosomal characteristic proteins, namely TSG101, CD9, syntenin, and calnexin. Employ RIPA lysis buffer to extract the total protein from exosomes, and utilize a BCA kit (P0011/Beyotime, Shanghai, China) to quantify the protein concentration. Protein (20 μg) was separated by 12% SDS-PAGE and transferred onto PVDF membranes (FPV403030/JET BIOFIL, Guangzhou, China). After blocking the membrane with milk, cut it as needed. Rabbit anti-TSG101 (ab125011/Abcam, Shanghai, China) (1:1000), rabbit anti-CD9 (BM4212/Bosterbio, Wuhan, China) (1:1000), rabbit anti-syntenin (ab19903/Abcam, Shanghai, China) (1:1000) and rabbit anti-calnexin (12186/SAB, Maryland, USA) (1:1000) were co-incubated with the PVDF membrane and slowly shaken at 4°C overnight. Dilute the HRP-conjugated goat anti-rabbit IgG (H + L) secondary antibody (31460/Invitrogen, Shanghai, China) at 1:5000 in a 5% skim milk TBST solution, immerse the membrane in the secondary antibody solution, and incubate at room temperature for 1 h. The proteins were identified using an ECL Plus chemiluminescent kit (1810212/Clinx, Shanghai, China). Finally, place the membrane in a chemiluminescence gel imaging system (ChemiScope 3000mini/Clinx, Shanghai, China) to photograph and save the images.

2.7 | Urinary exosome RNA extraction and sequencing

Exosome extraction and sequencing were carried out at Kangcheng Biotechnology Co. Ltd., Shanghai. In accordance with the manufacturer's instructions, the NEB Multiplex Small RNA Library Prep Set from Illumina was utilized to fabricate sequencing libraries. Subsequently, the quality of these libraries was evaluated using the Agilent 2100 Bioanalyzer. Mixed sequencing libraries derived from different samples were denatured with 0.1M NaOH to yield single-stranded DNA, which was then sequenced on an Illumina sequencer.

2.8 | Receiver operating characteristic curve (ROC)

The diagnostic value of the urinary exosomal miRNA network in IgA vasculitis nephritis (IgAVN) was appraised via the receiver operating characteristic (ROC) curve. A *p*-value less than .05 was considered to denote a statistically significant difference.

2.9 | miRNA-mRNA network construction

The target genes of miRNAs were predicted. To predict the target relationships between miRNAs and genes, the miRTarBase was employed. Subsequently, Cytoscape was utilized to construct a visual network graph.

2.10 | Gene function and metabolic pathway analysis

Gene function and metabolic pathway analyses were conducted via the Enrichr platform. Findings with a *p*-value threshold below .05 were considered to signify significant enrichment.

2.11 | Data statistical analysis

In this study, all data were subjected to statistical analysis using SPSS 25.0 software and R language version 4.1.2. Quantitative data that adhered to a normal distribution were presented as the mean ± standard deviation (±*s*). For inter-group comparisons of such data, the independent-samples *t* test was employed in parametric testing, assuming equal variances and a normal distribution of values in both groups. Conversely, quantitative data not conforming to a normal distribution were depicted as the median *M* (*Q*1, *Q*3). For inter-group comparisons of these data, the Mann–Whitney *U* test was utilized in non-parametric testing, and correlation analysis was carried out using the Spearman method.

3 | RESULTS

3.1 | Clinical information

This study encompassed a total of 5 children with IgA vasculitis (IgAV) and 5 children with IgA vasculitis nephritis (IgAVN), with each group consisting of 3 males and 2 females. The mean age of the IgAV group was (8.4 ± 3.1) years, while that of the IgAVN group was (8.2 ± 1.8) years (Table 1). Among the 5 children with IgAVN, the renal pathology was classified as grade IIA in 1 case, grade IIIA in 2 cases, and grade IIIB in 2 cases (Table 2).

3.2 | Identification of urinary exosomes

Under the TEM, exosomes were observed as round-shaped small vesicles with characteristic double membrane structures (Figure 1A). Using nanoparticle tracking analysis (NTA) to conduct particle size analysis on exosomes, the results showed that the particle size conformed to the size characteristics of exosomes, with a size range of 30–150 nm and an average size of (75.8 ± 13.3) nm (Figure 1B). The particle concentration was 4.83×10^{11} particles/mL (Figure 1C). BCA assay results indicated that the concentration of urinary exosome proteins was 0.875527 μg/μL. Western Blot (WB) results showed that the extracted exosomes contained the positive proteins TSG101, CD9, and syntenin, while the negative protein calnexin was not detected (Figure 1D).

4 | ANALYSIS OF URINARY EXOSOME miRNA SEQUENCING RESULTS

4.1 | Differential expression of urinary exosome miRNA between IgAVN and IgAV groups

After extracting total RNA from each sample individually to construct distinct sequencing libraries, raw data for each sample were generated independently on the Illumina sequencer. The raw data underwent quality control measures, filtering, and trimming procedures. Subsequently, they were aligned with the reference genome. Data sets demonstrating favorable alignment results were then analyzed to determine miRNA

TABLE 1 General information of IgAV group and IgAVN group.

	IgAV group	IgAVN group	*p*
Age (years)	8.4 ± 3.1	8.2 ± 1.8	.868
M: F	3:2	3:2	1.000
Serum creatinine (μmol/L)	45.7 (37.8, 48.8)	37.8 (35.6, 64.9)	.917
Urinary red blood cells (per high-power field)	2	5 (2, 14)	.054
Urinary protein levels (g/24 h)	0.06 (0.035, 0.08)	0.34 (0.07, 0.90)	.049
eGFR (mL/min/1.73 m^2)	196.78 ± 40.83	194.20 (140.00, 232.4)	.917

expression levels. The number of miRNAs that aligned with the known miRNA database was 708 in the IgAVN group and 677 in the IgAV group. A total of 589 exosomal miRNAs were commonly expressed between the two groups; specifically, 119 were uniquely expressed in the IgAVN group and 88 were uniquely expressed in the IgAV group. EdgeR software was used to analyze the differential expression of all exosomal miRNAs detected in urine samples of IgAV and IgAVN children. Results were filtered using a *p*-value cut-off of less than 0.05. This filtering process identified 57 differentially expressed miRNAs. Among these, 42 were upregulated and 15 were downregulated in the IgAVN group (Figure 2A). The top 10 significantly upregulated miRNAs and the top 10 significantly downregulated miRNAs are presented in Figure 2B.

TABLE 2 Renal pathological data of the IgAVN group.

Scoring categories	*n* (%)
Class I	0 (0)
Class II, Type A	1 (20)
Class II Type B	0 (0)
Class III, Type A	2 (40)
Class III B	2 (40)
Class IV	0 (0)
Class V	0 (0)
VI	0 (0)

4.2 | Lasso regression analysis

Lasso regression analysis was performed on the 57 differentially expressed miRNAs. Employing the minimum lambda criterion, 8 miRNAs exhibiting the highest correlation with IgAVN were identified (Figure 3A,B). These miRNAs were hsa-miR-3065-5p, hsa-miR-383-5p, hsa-miR-25-3p, hsa-miR-186-3p, hsa-miR-450b-5p, hsa-miR-204-5p, hsa-miR-200b-3p, and hsa-miR-499a-5p (Figure 3C and Table 3). Among them, hsa-miR-3065-5p, hsa-miR-383-5p, and hsa-miR-25-3p were upregulated in the IgAVN group, whereas hsa-miR-186-3p, hsa-miR-450b-5p, hsa-miR-204-5p, hsa-miR-200b-3p, and hsa-miR-499a-5p were downregulated. A heatmap illustrated that these 8 miRNAs could precisely discriminate between the IgAV and IgAVN groups (Figure 4).

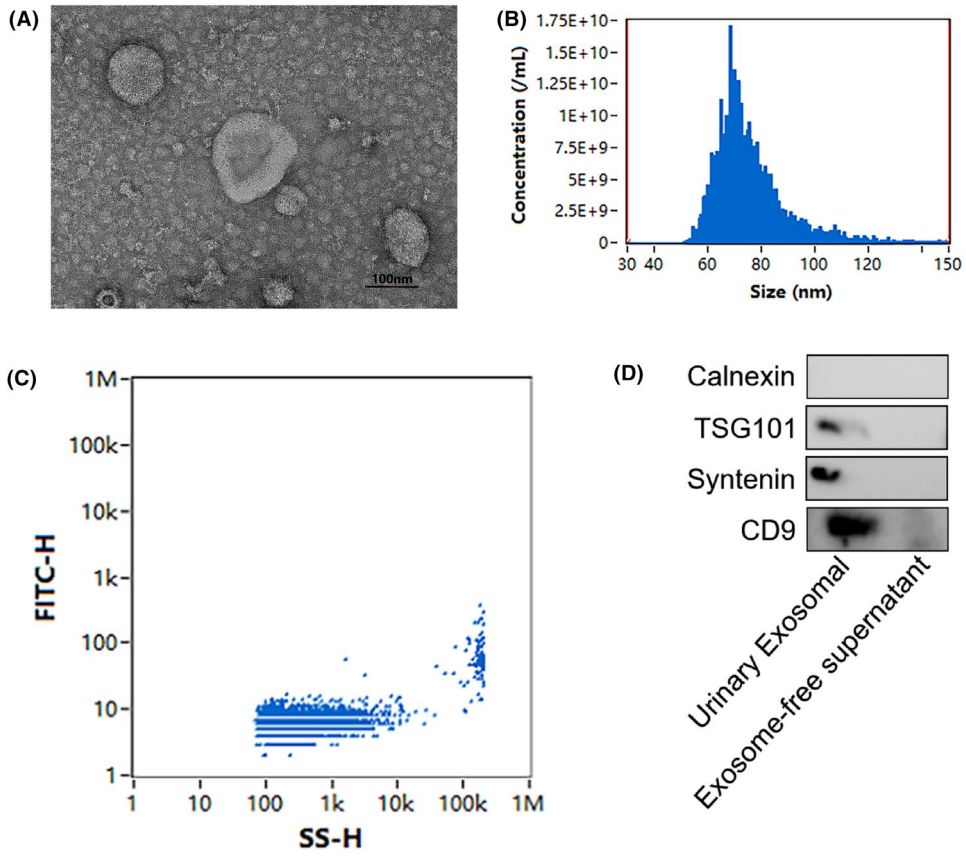

FIGURE 1 (A) Transmission electron microscopy image of urinary exosomes. (B) Schematic diagram of urinary exosome particle size. (C) Schematic diagram of exosome concentration. (D) Identification of characteristic proteins of urinary exosomes.

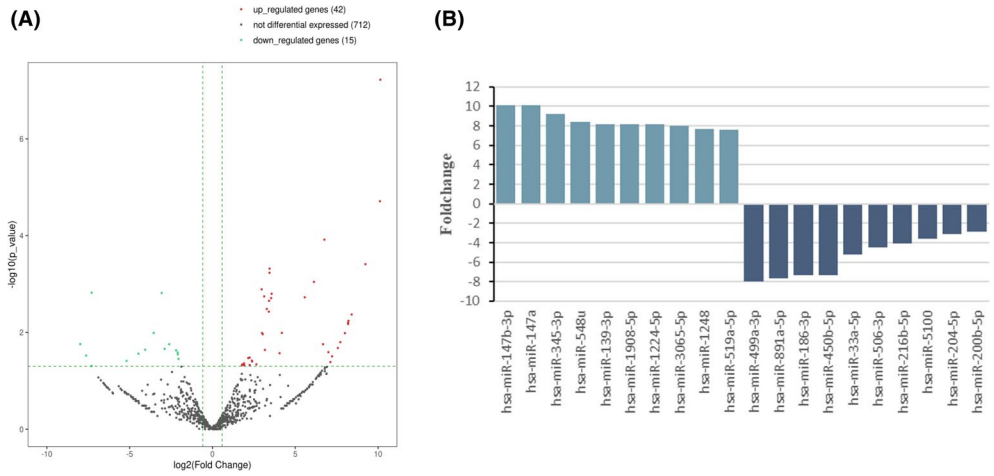

FIGURE 2 (A) Volcano plot of differential urinary exosomal miRNAs between the IgAVN and IgAV groups, where red dots represent upregulated exosomal miRNAs, green dots represent downregulated miRNAs, and black dots represent non-differential expressed miRNAs. (B) The top 10 upregulated and the top 10 downregulated differential miRNAs.

4.3 | ROC curve analysis

We utilized ROC curve analysis to assess the diagnostic value of the aforementioned miRNAs in IgAVN (Figure 5). The *AUC* and *P* values are as follows (Table 4): hsa-miR-3065-5p: AUC = 1.0, $p = .009$; hsa-miR-383-5p: AUC = 0.9, $p = .037$; hsa-miR-25-3p: AUC = 0.96, $p = .016$; hsa-miR-186-3p: AUC = 0.795, $p = .296$; hsa-miR-450b-5p: AUC = 1.0, $p = .009$; hsa-miR-204-5p: AUC = 0.8, $p = .117$; hsa-miR-200b-3p: AUC = 0.8, $p = .117$; hsa-miR-499a-5p: AUC = 0.92, $p = .028$. The results indicate that a total of 5 miRNAs have diagnostic value in IgAVN, which are hsa-miR-3065-5p, hsa-miR-383-5p, hsa-miR-25-3p, hsa-miR-450b-5p, and hsa-miR-499a-5p.

4.4 | Investigation of candidate miRNAs' target genes

The miRTarBase website was employed to predict the target genes of the five selected candidate miRNAs. To guarantee the reliability of the results, the findings were further validated using two additional websites, TargetScan and miRDB. In the end, 95 target genes predicted for the five candidate miRNAs were identified.

To clarify the biological functions of the 95 IgAVN-related target genes, gene function and metabolic pathway analyses were performed via the Enrichr database. The gene function analysis revealed that the biological processes (BP) corresponding to the target genes of upregulated miRNAs were enriched in Intrinsic Apoptotic Signaling Pathway In Response To DNA Damage By P53 Class Mediator, Regulation Of Glial Cell Differentiation, Ras Protein Signal Transduction, Positive Regulation Of Arp2/3 Complex-Mediated Actin Nucleation, and Intrinsic Apoptotic Signaling Pathway By P53 Class Mediator (Figure 6A). The cellular components (CC) were enriched in Platelet Alpha Granule, Exocytic Vesicle Membrane, Synaptic Vesicle Membrane, Cdc73/Paf1 Complex, and Neuronal Dense Core Vesicle (Figure 6B). The molecular functions (MF) were enriched in Ubiquitin-Protein Transferase Activity, Ubiquitin Protein Ligase Activity, Protease Binding, Ubiquitin-Like Protein Ligase Activity, and Nucleosome Binding (Figure 6C). The BP corresponding to downregulated miRNA target genes were enriched in Negative Regulation Of Cardiac Muscle Cell Differentiation, Pituitary Gland Development, Regulation Of Vascular Associated Smooth Muscle Cell Apoptotic Process, Regulation Of Vascular Associated Smooth Muscle Cell Differentiation, and Positive Regulation Of Protein K63-linked Ubiquitination (Figure 7A). The CC were enriched in G Protein-Coupled Receptor Dimeric Complex, Nucleus, Intracellular Membrane-Bounded Organelle, Azurophil Granule Membrane, and Voltage-Gated Potassium Channel Complex (Figure 7B). The MF were enriched in Leucine Binding, Transcription Regulatory Region Nucleic Acid Binding, GABA Receptor Activity, miRNA Binding, and Amino Acid Binding (Figure 7C). Metabolic pathway analysis revealed that the target genes corresponding to upregulated miRNAs were enriched in Pleural Mesothelioma, Apoptosis, miRNA Targets In ECM And Membrane Receptors, TGF Beta Signaling Pathway, and Caloric Restriction And Aging (Figure 6D). The target genes corresponding to downregulated miRNAs were enriched in Mesodermal Commitment Pathway, Cell Lineage Map For Neuronal Differentiation, Endoderm Differentiation, Let 7 Inhibition Of ES Cell

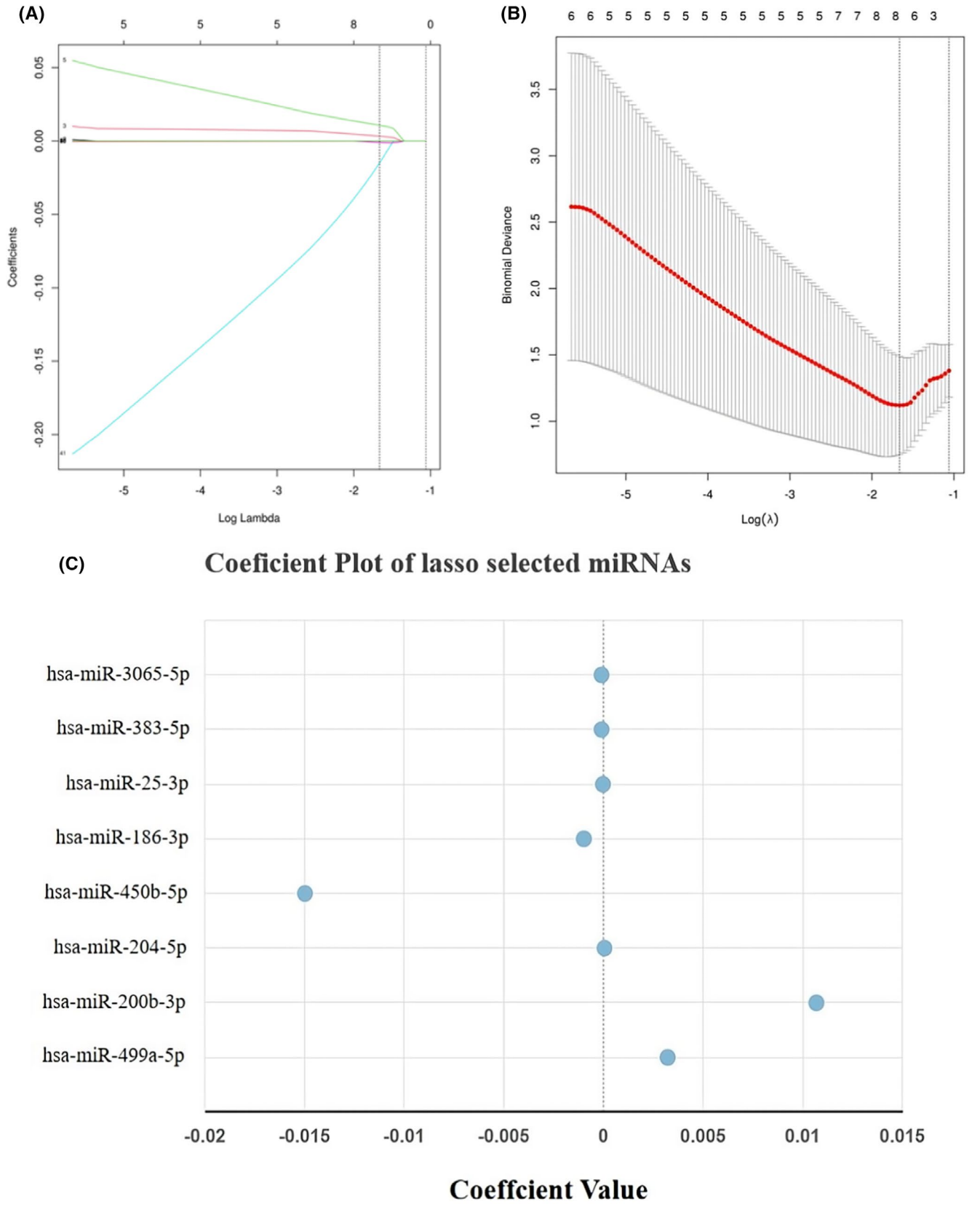

FIGURE 3 (A) Path diagram of the coefficients from the LASSO regression analysis of differential miRNAs. (B) Cross-validation curve. (C) Plot of regression coefficients.

Reprogramming, and GPCRs Class C Metabotropic Glutamate Pheromone (Figure 7D).

4.5 | Construction of the exosomal miRNA-mRNA network and functional enrichment analysis

The protein–protein interaction (PPI) network of IgAVN-associated target genes was constructed using the STRING database (Figure 8A), and subsequently visualized using Cytoscape software (Figure 8B). Based on this PPI network, we utilized the Cytohubba plugin within Cytoscape software to identify the top 10 hub genes in the network, which are IRF1, IGF1, COL1A2, SP1, TP53, CHD4, GATAD2B, SOX2, THBS1, and ITGA1 (Figure 8C). Finally, an miRNA-hub gene network was established using Cytoscape software, resulting in the construction of an exosomal miRNA-mRNA network composed of 4 key miRNAs (hsa-miR-3065-5p, hsa-miR-383-5p, hsa-miR-25-3p, hsa-miR-450b-5p) and 10 hub mRNAs (ITGA1, THBS1, CHD4, TP53, IRF1, SP1, IGF1, COL1A2, GATAD2B, SOX2) (Figure 8D and Table 5). These selected miRNAs and mRNAs are key exosomal miRNAs and RNA interaction hubs that may play a significant role in the pathogenesis and progression of IgAVN through exosomal mechanisms (Table 6).

Subsequently, we utilized the Enrichr database to perform gene function and metabolic pathway analysis on the identified 10 hub genes. The gene function analysis revealed that the biological processes (BP) of these 10 hub genes were enriched in Positive Regulation of Nucleic Acid-Templated Transcription, Negative Regulation of Cell Population Proliferation, Positive Regulation Of DNA-templated Transcription, Regulation Of Cell Population Proliferation, and Regulation Of Cell Fate Commitment. The cellular components (CC) were enriched in Platelet Alpha Granule Lumen, Platelet Alpha Granule, Exocytic Vesicle, Secretory Vesicle, and Endoplasmic Reticulum Lumen. The molecular functions

TABLE 3 Table of LASSO regression coefficients for differential miRNAs.

miRNA	Coeff_min_lamda
hsa-miR-3065-5p	.0032
hsa-miR-383-5p	.0106
hsa-miR-25-3p	.0005
hsa-miR-186-3p	−.1497
hsa-miR-450b-5p	−.0009
hsa-miR-204-5p	−1.9316
hsa-miR-200b-3p	−9.0729
hsa-miR-499a-5p	−9.2675

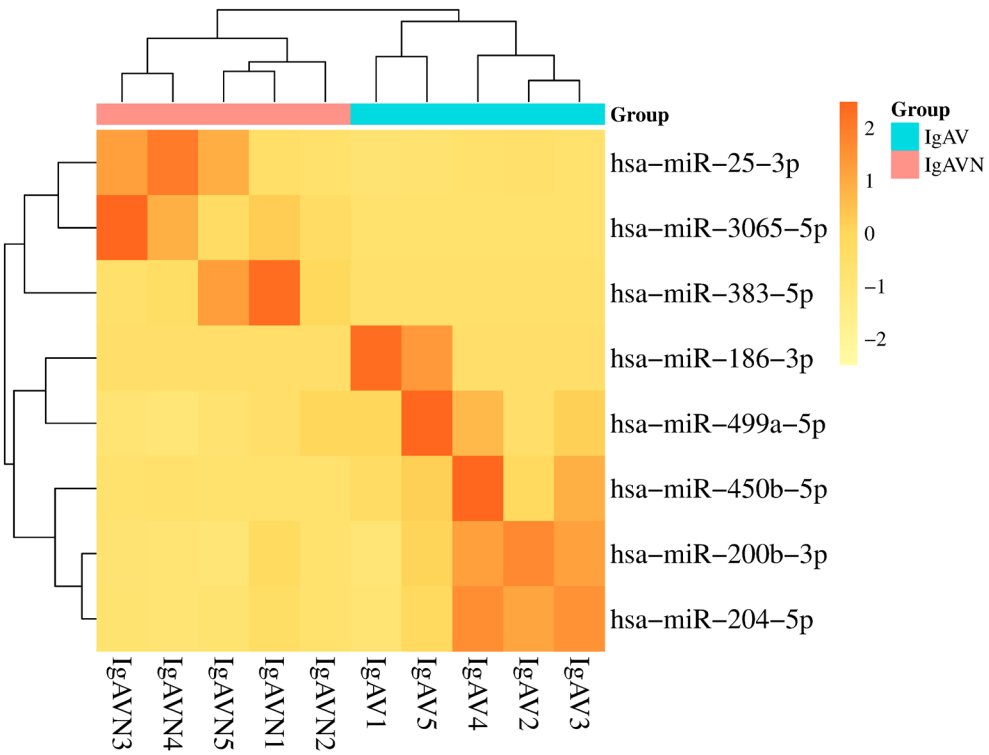

FIGURE 4 Hierarchical clustering heatmap of differential miRNAs, where each column represents a sample and each row represents a miRNA, with the dendrogram on the left representing gene clustering.

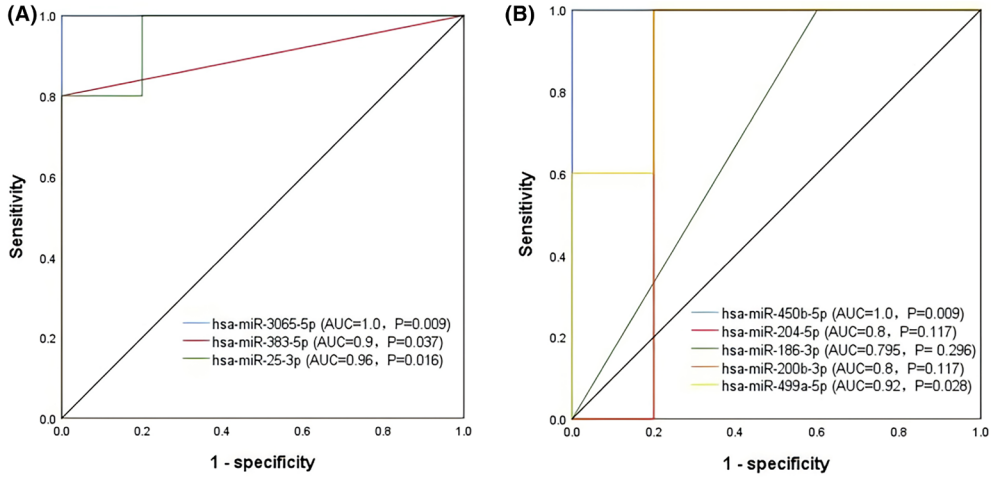

FIGURE 5 (A) ROC curve analysis of upregulated miRNAs in the IgAVN group. (B) ROC curve analysis of downregulated miRNAs in the IgAVN group.

TABLE 4 Results of ROC curve analysis.

miRNA	AUC	*p*	95% CI
hsa-miR-3065-5p	1.000	.009	1.000
hsa-miR-383-5p	0.900	.037	0.675–1.000
hsa-miR-25-3p	0.960	.016	0.675–1.000
hsa-miR-186-3p	0.795	.296	0.675–1.000
hsa-miR-450b-5p	1.000	.009	1.000
hsa-miR-204-5p	0.800	.117	0.449–1.000
hsa-miR-200b-3p	0.800	.117	0.449–1.000
hsa-miR-499a-5p	0.920	.028	0.738–1.000

(MF) were enriched in Protease Binding, Nucleosomal DNA Binding, Transcription Regulatory Region Nucleic Acid Binding, Nucleosome Binding, and DNA Binding. Metabolic pathway analysis indicated that the pathways enriched for these 10 hub genes were miRNA Targets In ECM And Membrane Receptors, PI3K Akt Signaling, TGF Beta Signaling Pathway, Focal Adhesion, and IL18 Signaling (Figure 9).

4.6 | Correlation analysis between urinary exosomal miRNAs and clinical parameters

We analyzed the correlation between the aforementioned five urinary exosomal miRNAs and clinical parameters in children with IgAVN. There was no correlation found between hsa-miR-3065-5p, hsa-miR-25-3p, hsa-miR-450b-5p, and hsa-miR-499a-5p with serum creatinine, urinary red blood cells, urinary protein, eGFR, and pathological grading. Hsa-miR-383-5p showed a negative correlation with proteinuria levels ($r=-.9$, $p=.04$) and no correlation with serum creatinine, urinary red blood cells, eGFR, or pathological grading (Table 7).

5 | DISCUSSION

IgAV represents the most prevalent form of systemic vasculitis during childhood, with an overall incidence that is on the rise.[10] The severity of kidney damage represents the most pivotal factor influencing the prognosis of IgAV.[11] Consequently, the early identification of IgAV kidney injury and the implementation of corresponding therapeutic measures are of paramount importance for enhancing the prognosis of children with IgAV. Renal biopsy, serving as the gold standard for the diagnosis of IgAVN, has its clinical application restricted owing to its invasive character, poor repeatability, and low patient compliance. Traditional blood and urine tests exhibit a lag effect, and the previously reported early predictive markers fail to meet the criteria of high specificity, high sensitivity, and ease of detection. Thus, there is an urgent necessity for novel biomarkers for the diagnosis of IgAV kidney damage. Urinary exosomal miRNAs, resembling kidney tissue miRNAs, are capable of reflecting the physiological and pathological state of the kidney. Their characteristics, including easy accessibility, non-invasiveness, high sensitivity, and high specificity, render them extensively utilized in the screening of biomarkers for kidney diseases. Therefore, this study endeavors to identify biomarkers for IgAV kidney damage from the perspective of urinary exosomal miRNAs, with the anticipation of providing new indicators for the non-invasive diagnosis of IgAV kidney damage.

In this study, high-throughput miRNA sequencing technology was utilized to investigate the urinary exosomal

profiles of children with IgAV and IgAVN. As a result, 57 differentially expressed miRNAs were identified, among which 42 were upregulated and 15 were downregulated in the IgAVN group. Subsequently, through the integration of Lasso regression analysis and ROC curve analysis, 5 candidate miRNAs closely associated with IgAVN were pinpointed, namely hsa-miR-3065-5p, hsa- miR-383-5p, hsa-miR-25-3p, hsa-miR-450b-5p, and hsa-miR-499a-5p. A substantial amount of research has been conducted on the functions and mechanisms of the aforementioned differentially expressed exosomal miRNAs in diseases. For example, hsa-miR-383-5p induces oxidative stress and apoptosis in rat hepatocytes by targeting and suppressing *Bcl2* translation[12]; hsa-miR-25-3p has the capacity to mediate inflammatory responses via the PTEN/PI3K/AKT/NF-κB pathway and is additionally involved in the progression of diabetic nephropathy through the regulation of cell proliferation and apoptosis.[13,14] Considering that the activation of renal glomerular inflammation in IgAVN contributes to glomerular damage, the identification of these miRNAs provides novel perspectives on the pathophysiological processes of renal damage in IgAVN.

To delve deeper into the potential functions of these differentially expressed miRNAs in the pathogenesis of IgAVN, a PPI network was constructed for their corresponding 95 target genes by means of the STRING database. Subsequently, key modules within this network were identified through the utilization of the Cytohubba plugin in Cytoscape software. Finally, an exosomal miRNA-mRNA network was established based on this key module, encompassing 4 key miRNAs (hsa-miR-3065-5p, hsa-miR-25-3p, hsa-miR-383-5p, hsa-miR-450b-5p) and 10 hub mRNAs (ITGA1, THBS1, CHD4, TP53, IRF1, SP1, IGF1, COL1A2, GATAD2B, SOX2). Notably, prior research has also uncovered the potential functions of the aforementioned hub genes in the pathogenesis of kidney-related disorders. For instance, Sun et al. reported that *THBS1* is highly expressed in sepsis-induced AKI patients, and the knockdown of *THBS1* contributes to the reduction of cellular inflammatory necrosis and the improvement of AKI conditions.[15] In the context of diabetic nephropathy, circular RNA circUBXN7 is upregulated under the influence of *SP1*, leading to macrophage infiltration, fibrosis, and the generation of proteinuria.[16] Moreover, Gholaminejad et al. detected the involvement of *TP53* in the pathogenesis of IgAN, and Liu et al. hypothesized that Shenbing Decoction II could treat IgAN by targeting the TP53 protein.[17,18] These findings imply that the four identified key miRNAs might play a substantial role in the renal damage process of IgAVN.

To further expound upon the biological functions of the differentially expressed urinary exosomes, bioinformatics analysis was carried out. The gene function analysis results indicated that the genes encoding these 10 hub mRNAs were enriched in positive regulation of nucleic acid-templated transcription, platelet alpha granule, and protease binding; metabolic pathway analysis showed enrichment in targets of miRNAs in the extracellular matrix and membrane receptors, the PI3KAkt signaling pathway, and the TGF-β signaling pathway. Studies have shown that platelet alpha granules can induce glomerular mesangial cell migration, and the platelet-derived growth factors released are key drivers of renal fibrosis.[19,20] Other investigations have demonstrated that in IgAV patients with renal involvement, there exists a dysregulation of excessive extracellular matrix deposition, which represents one of the hallmarks of renal fibrosis.[21,22] Moreover, this study identified two classic pathways, namely the PI3K-Akt signaling pathway and the TGF-β signaling pathway, that are enriched in inflammation and profibrotic processes. The PI3K-Akt signaling pathway is implicated in regulating cell survival, migration, and metabolism, and it plays a role in angiogenesis and the recruitment of inflammatory factors.[23] Inhibition of the PI3K-Akt signaling pathway can mitigate the degree of renal fibrosis, as well as reduce neutrophil infiltration and the release of key inflammatory factors in renal tissue.[24,25] TGF-β is also a major factor leading to renal fibrosis and can promote fibrotic transformation of renal mesangial cells through the Smad2/3/YAP signaling axis, participating in key pathological processes in the progression of chronic kidney disease, such as fibroblast proliferation, epithelial-to-mesenchymal transition, and extracellular matrix production.[26–28] Inhibition of the TGF-β subtype, TGF-β1, or its downstream signaling pathway can significantly curtail renal fibrosis.[29] The aforementioned studies imply that urinary exosomal miRNAs in children with IgAVN are enriched in renal fibrosis and inflammation-related pathways, potentially facilitating a better understanding of the pathogenesis of IgAVN.

To further explore the association between the aforementioned differentially expressed urinary exosomal miRNAs and the clinical manifestations of children

FIGURE 6 Utilization of the Enrichr database for the functional and metabolic pathway analysis of target genes associated with upregulated miRNAs. (A) Analysis of biological processes. (B) Analysis of cellular components. (C) Analysis of molecular functions. (D) Metabolic pathway analysis.

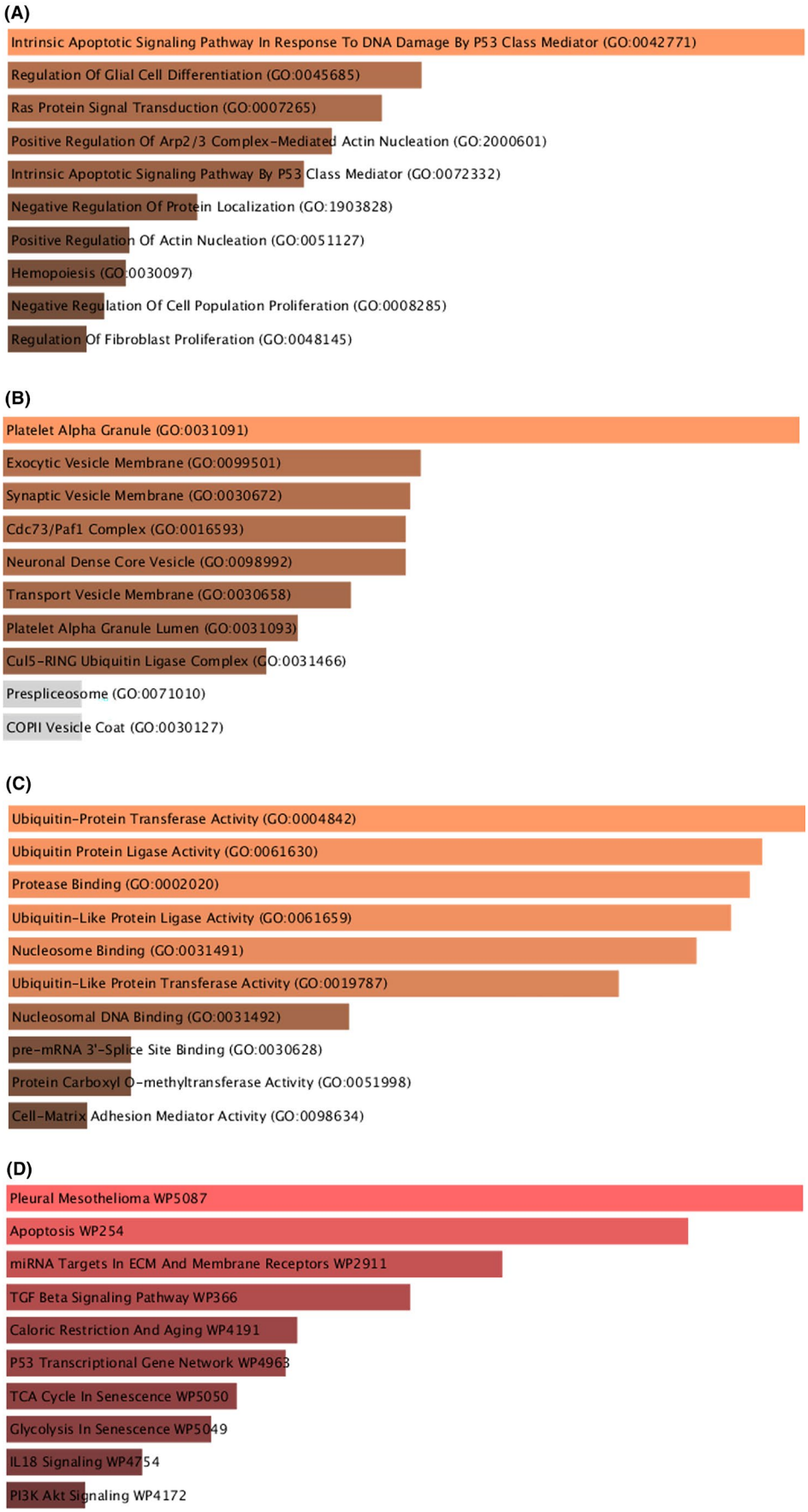
(A)
Intrinsic Apoptotic Signaling Pathway In Response To DNA Damage By P53 Class Mediator (GO:0042771)
Regulation Of Glial Cell Differentiation (GO:0045685)
Ras Protein Signal Transduction (GO:0007265)
Positive Regulation Of Arp2/3 Complex-Mediated Actin Nucleation (GO:2000601)
Intrinsic Apoptotic Signaling Pathway By P53 Class Mediator (GO:0072332)
Negative Regulation Of Protein Localization (GO:1903828)
Positive Regulation Of Actin Nucleation (GO:0051127)
Hemopoiesis (GO:0030097)
Negative Regulation Of Cell Population Proliferation (GO:0008285)
Regulation Of Fibroblast Proliferation (GO:0048145)
(B)
Platelet Alpha Granule (GO:0031091)
Exocytic Vesicle Membrane (GO:0099501)
Synaptic Vesicle Membrane (GO:0030672)
Cdc73/Paf1 Complex (GO:0016593)
Neuronal Dense Core Vesicle (GO:0098992)
Transport Vesicle Membrane (GO:0030658)
Platelet Alpha Granule Lumen (GO:0031093)
Cul5-RING Ubiquitin Ligase Complex (GO:0031466)
Prespliceosome (GO:0071010)
COPII Vesicle Coat (GO:0030127)
(C)
Ubiquitin-Protein Transferase Activity (GO:0004842)
Ubiquitin Protein Ligase Activity (GO:0061630)
Protease Binding (GO:0002020)
Ubiquitin-Like Protein Ligase Activity (GO:0061659)
Nucleosome Binding (GO:0031491)
Ubiquitin-Like Protein Transferase Activity (GO:0019787)
Nucleosomal DNA Binding (GO:0031492)
pre-mRNA 3'-Splice Site Binding (GO:0030628)
Protein Carboxyl O-methyltransferase Activity (GO:0051998)
Cell-Matrix Adhesion Mediator Activity (GO:0098634)
(D)
Pleural Mesothelioma WP5087
Apoptosis WP254
miRNA Targets In ECM And Membrane Receptors WP2911
TGF Beta Signaling Pathway WP366
Caloric Restriction And Aging WP4191
P53 Transcriptional Gene Network WP4963
TCA Cycle In Senescence WP5050
Glycolysis In Senescence WP5049
IL18 Signaling WP4754
PI3K Akt Signaling WP4172

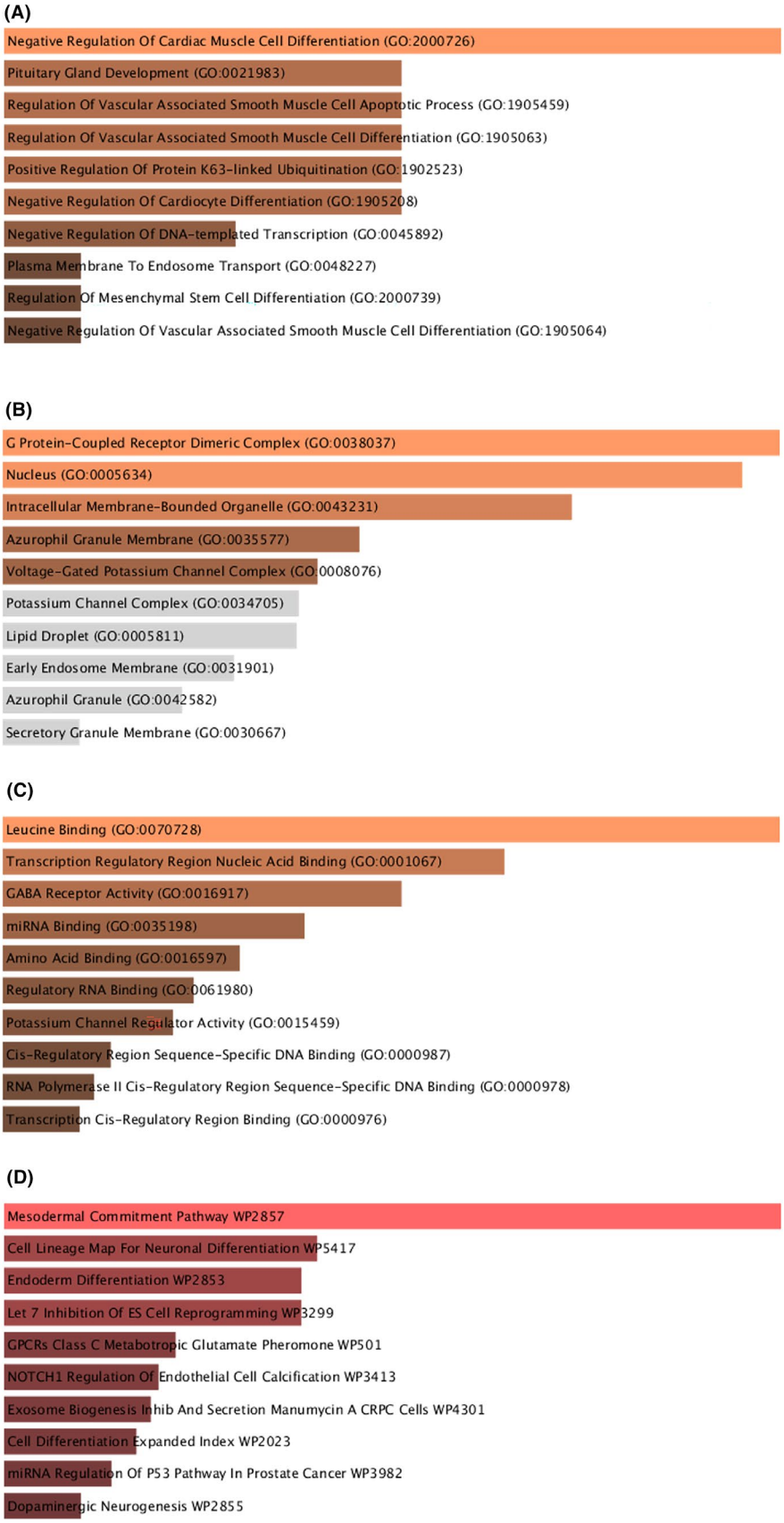

FIGURE 7 Utilization of the Enrichr database for the functional and metabolic pathway analysis of target genes associated with downregulated miRNAs. (A) Analysis of biological processes. (B) Analysis of cellular components. (C) Analysis of molecular functions. (D) Metabolic pathway analysis.

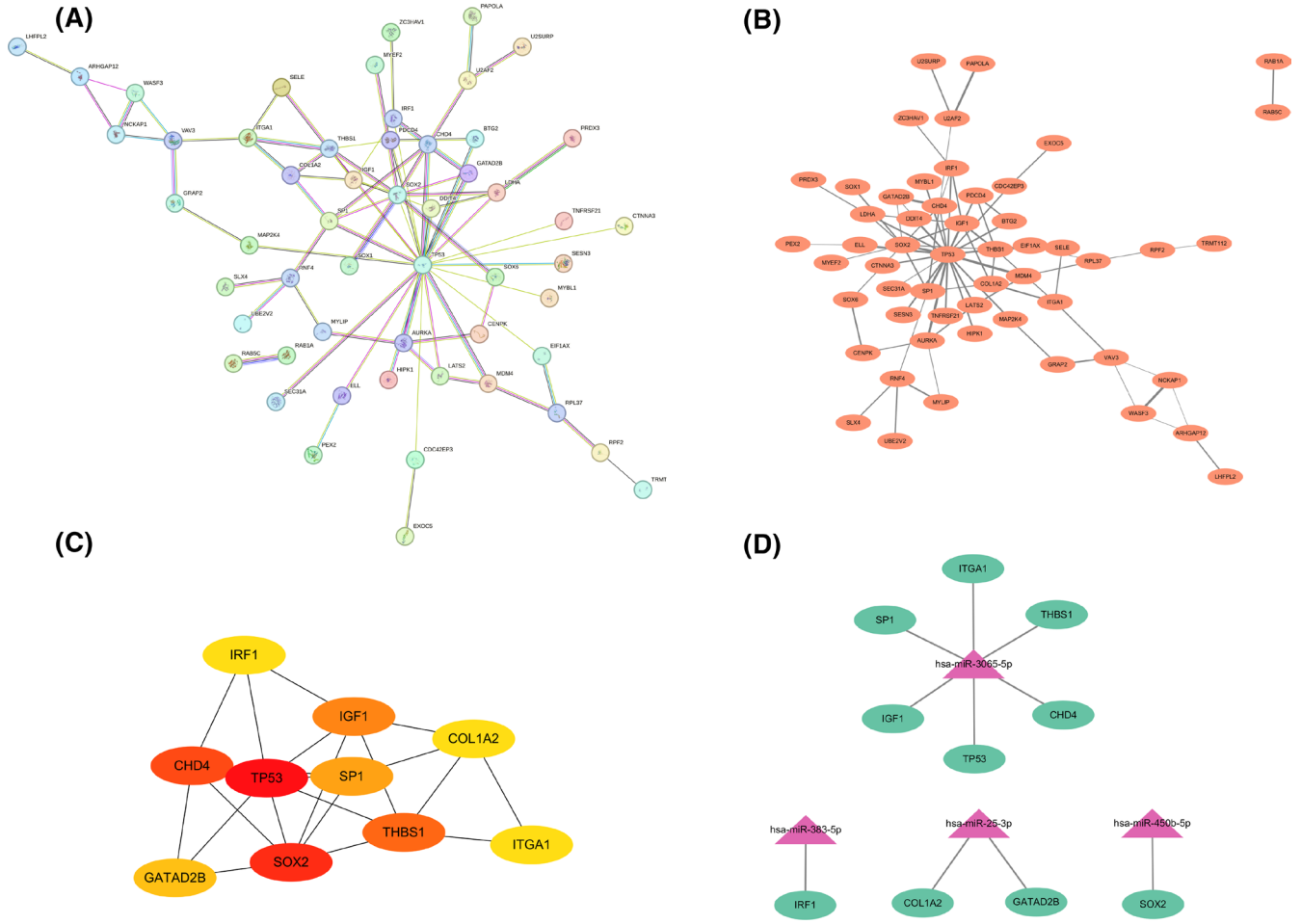

FIGURE 8 (A) Analysis of the PPI network for 95 target genes of 5 exosomal miRNAs using the STRING database; (B) Analysis of the PPI network using Cytoscape software; (C) Identification of the top 10 hub genes using the Cytohubba plugin in Cytoscape software; (D) MiRNA-hub gene network, where green ellipses represent hub genes and purple triangles represent key miRNAs.

TABLE 5 Details of the top 10 hub genes.

Sequence	Gene	Description
1	*IRF1*	Interferon regulatory factor 1
2	*IGF1*	Insulin like growth factor 1
3	*COL1A2*	Collagen type I alpha 2 chain
4	*SP1*	Sp1 transcription factor
5	*TP53*	Tumor protein p53
6	*CHD4*	Chromodomain helicase DNA binding protein 4
7	*GATAD2B*	GATA zinc finger domain containing 2B
8	*SOX2*	SRY-box transcription factor 2
9	*THBS1*	Thrombospondin 1
10	*ITGA1*	Integrin subunit alpha 1

TABLE 6 List of 4 key exosomal miRNAs.

miRNA	mRNA count	mRNA
hsa-miR-3065-5p	6	ITGA1, THBS1, CHD4, TP53, IGF1, SP1
hsa-miR-25-3p	2	COL1A2, GATAD2B
hsa-miR-383-5p	1	IRF1
hsa-miR-450b-5p	1	SOX2

with IgAVN, a correlation analysis was performed. The analysis revealed that exosomal hsa-miR-383-5p was significantly correlated with proteinuria levels ($r = -0.9$, $p = .04$). Given that renal involvement represents the primary characteristic of IgAVN, and proteinuria levels are

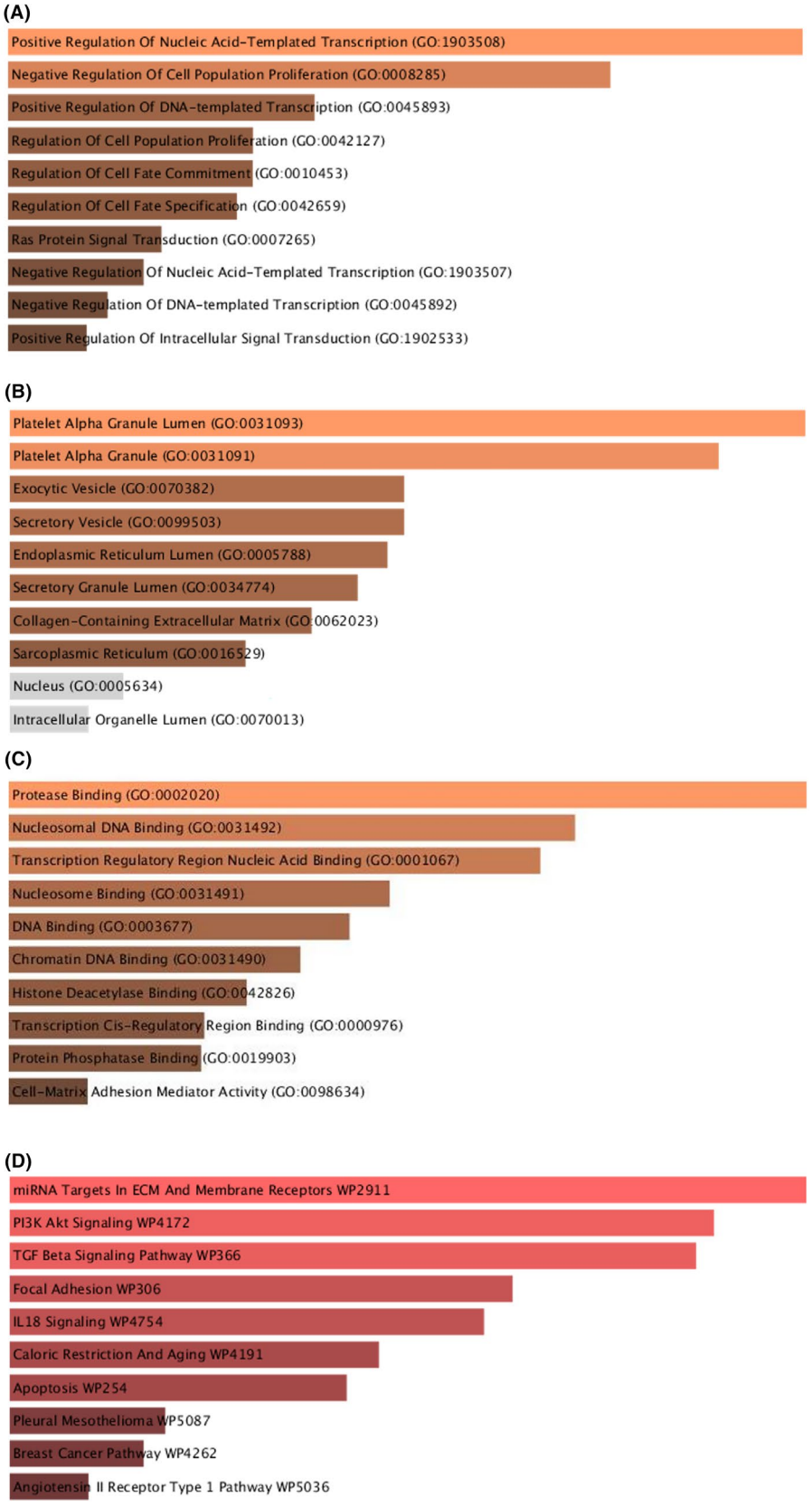

FIGURE 9 Utilization of the Enrichr database for gene function and metabolic pathway analysis of the 10 hub genes. (A) Biological process. (B) Cellular component. (C) Molecular function. (D) Metabolic pathway analysis.

TABLE 7 Correlation analysis between five miRNAs and clinical parameters of IgAVN.

	hsa-miR-3065-5p		hsa-miR-383-5p		hsa-miR-25-3p		hsa-miR-450b-5p		hsa-miR-499a-5p	
Clinical parameters	***r***	***p***	***r***	***p***	***r***	***p***	***r***	***p***	***r***	***p***
Serum creatinine	−.49	.94	−.50	.39	1.00	.84	−.30	.62	−.19	.75
Urinary red blood cells	.30	.62	−.10	.84	.00	1.00	.40	.51	.00	1.00
Urinary protein levels	.70	.19	−.90	.04	.80	.10	−.60	.29	−.80	.10
eGFR	.61	.27	−.04	.99	.04	.94	.40	.51	−.32	.60
Grade of pathology	.32	.60	.33	.53	.50	.39	−0.21	.73	−.78	.12

closely associated with the severity of kidney disease, with 24-h urinary protein regarded as the gold standard for proteinuria quantification, urinary exosomal hsa-miR-383-5p may potentially serve as a non-invasive biomarker for evaluating the disease status of IgAVN. However, it is noteworthy that in our cohort, the expression levels of hsa-miR-383-5p in two IgAVN patients overlapped with those in IgAV group (Figure 4), suggesting potential biological variability in miRNA regulation. While group-level analysis demonstrated statistical significance, these observations highlight the necessity of interpreting hsa-miR-383-5p levels in conjunction with other clinical parameters and biomarkers rather than as a standalone diagnostic criterion. Meanwhile, as an exploratory investigation, this research was constrained by funding and time limitations, leading to a relatively small sample size. Future studies should aim to expand the sample size to enhance the reliability and validity of the findings. Moreover, this study predominantly concentrated on the diagnostic and disease-assessment values of urinary exosomal miRNAs. In the future, in vivo and in vitro experiments will be necessary to validate the functions and mechanisms of the four miRNAs in IgAVN.

6 | CONCLUSION

In this study, differential exosomal miRNAs and mRNAs associated with IgAVN were identified, and a corresponding exosomal miRNA-mRNA network was constructed. It was ascertained that hsa-miR-3065-5p, hsa-miR-383-5p, hsa-miR-25-3p, and hsa-miR-450b-5p are key miRNAs implicated in the pathogenesis of IgAVN. These miRNAs may potentially mediate the disease progression by targeting profibrotic and inflammatory pathways. Among them, exosomal hsa-miR-383-5p is the most promising candidate to serve as a novel non-invasive biomarker for evaluating the disease status of IgAVN. These findings offer novel perspectives on the non-invasive diagnosis and treatment of IgAVN.

AUTHOR CONTRIBUTIONS

Xiaojing Nie, Yunfan Zhang, and Huanhuan Yang designed research. Yunfan Zhang, Huanhuan Yang, Yi Chen, Yuxian Tang, and Junyan Chen analyzed data. Jun Huang, Ai Feng, Zengfeng Weng, Fenrong Li, Jinfeng Lin, Jingqi Xie, Chunfang Zhang, Jie Chen, and Chunlin Gao performed research and acquired data. Yunfan Zhang, Huanhuan Yang, Chunlin Gao, and Xiaojing Nie discussed the mechanism. Yunfan Zhang and Huanhuan Yang wrote the paper. All authors were involved in drafting and revising the manuscript.

ACKNOWLEDGMENTS

The authors gratefully acknowledge Dr. Yue Du from Shengjing Hospital Affiliated to China Medical University for her invaluable contributions to the mechanistic interpretation and assistance with the study.

FUNDING INFORMATION

This work was supported by Science and Technology Innovation Project of Fujian Province (Granting number: 2019Y9043) and Key Project of Social Development of Fujian Province of China (Granting numbers: 2019Y0069 and 2023Y0068).

DISCLOSURES

The authors have no competing interests to declare that are relevant to the content of this article.

DATA AVAILABILITY STATEMENT

The data that support the findings of this study are available on request from the corresponding author. The data are not publicly available due to privacy and ethical restrictions.

ETHICS APPROVAL

This study was performed in line with the principles of the Declaration of Helsinki. Approval was granted by the Ethics Committee of Fujian Medical University and 900th Hospital of PLA Joint Logistic Support Force (Nos. 2019-009 and 2023-081).

CONSENT TO PARTICIPATE

Written informed consent was obtained from the parents.

ORCID

Yunfan Zhang https://orcid.org/0009-0004-6033-6179
Huanhuan Yang https://orcid.org/0009-0004-7653-775X
Yi Chen https://orcid.org/0009-0006-1668-105X
Yuxian Tang https://orcid.org/0009-0001-4179-0446
Junyan Chen https://orcid.org/0009-0007-5915-9656
Jun Huang https://orcid.org/0009-0008-8949-4639
Ai Feng https://orcid.org/0009-0007-4424-8752
Zengfeng Weng https://orcid.org/0009-0004-1857-6216
Fenrong Li https://orcid.org/0009-0004-3058-2571
Jinfeng Lin https://orcid.org/0009-0005-5198-8869
Jingqi Xie https://orcid.org/0009-0000-8924-2820
Chunfang Zhang https://orcid.org/0009-0007-1731-6342
Jie Chen https://orcid.org/0009-0008-0970-4086
Chunlin Gao https://orcid.org/0000-0003-2469-7992
Xiaojing Nie https://orcid.org/0000-0002-3144-1437

REFERENCES

1. Pillebout E, Sunderkötter C. IgA vasculitis. *Semin Immunopathol*. 2021;43:729-738.
2. Piram M, Mahr A. Epidemiology of immunoglobulin A vasculitis (Henoch-Schönlein): current state of knowledge. *Curr Opin Rheumatol*. 2013;25:171.
3. Ozen S, Marks SD, Brogan P, et al. European consensus-based recommendations for diagnosis and treatment of immunoglobulin A vasculitis-the SHARE initiative. *Rheumatology (Oxford)*. 2019;58:1607-1616.
4. Chen JY, Mao JH. Henoch-Schönlein purpura nephritis in children: incidence, pathogenesis and management. *World J Pediatr*. 2015;11:29-34.
5. Williams CE, Toner A, Wright RD, et al. A systematic review of urine biomarkers in children with IgA vasculitis nephritis. *Pediatr Nephrol*. 2021;36:3033-3044.
6. Nüsken E, Weber LT. IgA vasculitis nephritis. *Curr Opin Pediatr*. 2022;34:209-216.
7. Pillebout E, Jamin A, Ayari H, et al. Biomarkers of IgA vasculitis nephritis in children. *PLoS One*. 2017;12:e0188718.
8. Sonoda H, Lee BR, Park KH, et al. miRNA profiling of urinary exosomes to assess the progression of acute kidney injury. *Sci Rep*. 2019;9:4692.
9. Cao Y, Shi Y, Yang Y, et al. Urinary exosomes derived circRNAs as biomarkers for chronic renal fibrosis. *Ann Med*. 2022;54:1966-1976.
10. Xu L, Li Y, Wu X. IgA vasculitis update: epidemiology, pathogenesis, and biomarkers. *Front Immunol*. 2022;13:921864.
11. Wang K, Sun X, Cao Y, et al. Risk factors for renal involvement and severe kidney disease in 2731 Chinese children with Henoch-Schönlein purpura: a retrospective study. *Medicine (Baltimore)*. 2018;97:e12520.
12. Xu B, Zang SC, Lang LM, et al. Down-regulation of miR-383-5p suppresses apoptosis in oxidative stress rat hepatocytes by targeting Bcl2. *J Anim Physiol Anim Nutr (Berl)*. 2020;104:1948-1959.
13. Kim MJ, Lim SG, Cho DH, et al. Regulation of inflammatory response by LINC00346 via miR-25-3p-mediated modulation of the PTEN/PI3K/AKT/NF-κB pathway. *Biochem Biophys Res Commun*. 2024;709:149828.
14. Chen H, Tian T, Wang D. Dysregulation of miR-25-3p in diabetic nephropathy and its role in inflammatory response. *Biochem Genet*. 2025;63:1635-1646.
15. Sun J, Ge X, Wang Y, et al. USF2 knockdown downregulates THBS1 to inhibit the TGF-β signaling pathway and reduce pyroptosis in sepsis-induced acute kidney injury. *Pharmacol Res*. 2022;176:105962.
16. Lin Z, Lv D, Liao X, et al. CircUBXN7 promotes macrophage infiltration and renal fibrosis associated with the IGF2BP2-dependent SP1 mRNA stability in diabetic kidney disease. *Front Immunol*. 2023;14:1226962.
17. Gholaminejad A, Gheisari Y, Jalali S, et al. Comprehensive analysis of IgA nephropathy expression profiles: identification of potential biomarkers and therapeutic agents. *BMC Nephrol*. 2021;22:137.
18. Liu H, Chen W, Tian C, et al. The mechanism of Shenbing Decoction II against IgA nephropathy renal fibrosis revealed by UPLC-MS/MS, network pharmacology and experimental verification. *Heliyon*. 2023;9:e21997.
19. Ostendorf T, Boor P, Van Roeyen CRC, et al. Platelet-derived growth factors (PDGFs) in glomerular and tubulointerstitial fibrosis. *Kidney Int Suppl*. 2011;2014(4):65-69.
20. Barnes JL, Hevey KA. Glomerular mesangial cell migration. Response to platelet secretory products. *Am J Pathol*. 1991;138:859-866.
21. Bajželj M, Hladnik M, Blagus R, et al. Deregulation in adult IgA vasculitis skin as the basis for the discovery of novel serum biomarkers. *Arthritis Res Ther*. 2024;26:85.
22. Sparding N, Neprasova M, Maixnerova D, et al. Unique biomarkers of collagen type III remodeling reflect different information regarding pathological kidney tissue alterations in patients with IgA nephropathy. *Biomolecules*. 2023;13:1093.
23. Karar J, Maity A. PI3K/AKT/mTOR pathway in angiogenesis. *Front Mol Neurosci*. 2011;4:51.
24. Ni Y, Zhang H, Xian Q, et al. RfxCas13d-mediated inhibition of Circ1647 alleviates renal fibrosis via PI3K/AKT signaling pathway. *Ren Fail*. 2024;46:2331612.
25. Yang H, Zhang H, Tian L, et al. Curcumin attenuates lupus nephritis by inhibiting neutrophil migration via PI3K/AKT/NF-κB signalling pathway. *Lupus Sci Med*. 2024;11:e001220.
26. Ji C, Zhang J, Shi H, et al. Single-cell RNA transcriptomic reveal the mechanism of MSC derived small extracellular vesicles against DKD fibrosis. *J Nanobiotechnology*. 2024;22:339.
27. Singh J, Jain A, Bhamra R, et al. The mechanistic role of different mediators in the pathophysiology of nephropathy: a review. *Curr Drug Targets*. 2023;24:104-117.

28. López-Hernández FJ, López-Novoa JM. Role of TGF-β in chronic kidney disease: an integration of tubular, glomerular and vascular effects. *Cell Tissue Res*. 2012;347:141-154.
29. Meng X-M, Nikolic-Paterson DJ, Lan HY. TGF-β: the master regulator of fibrosis. *Nat Rev Nephrol*. 2016;12:325-338.

SUPPORTING INFORMATION

Additional supporting information can be found online in the Supporting Information section at the end of this article.

How to cite this article: Zhang Y, Yang H, Chen Y, et al. Construction and diagnostic efficacy assessment of the urinary exosomal miRNA-mRNA network in children with IgA vasculitis nephritis. *The FASEB Journal*. 2025;39:e70492. doi:10.1096/fj.202403111R